Title

Axisymmetric Simulations of Cone Penetration in Biocemented Sands

Journal

Journal of Geotechnical and Geoenvironmental Engineering, 148(11)

ISSN

1090-0241

Authors

Kortbawi, Maya El

Moug, Diane M

Ziotopoulou, Katerina

et al.

Publication Date

2022-11-01

DOI

10.1061/(asce)gt.1943-5606.0002914

Peer reviewed

ASCE

Axisymmetric Simulations of Cone Penetration in Biocemented Sands

Maya El Kortbawi, S.M.ASCE[1]; Diane M. Moug, Ph.D., A.M.ASCE[2]; Katerina Ziotopoulou, Ph.D., P.E., M.ASCE[3]; Jason T. DeJong, Ph.D., F.ASCE[4]; and Ross W. Boulanger, Ph.D., P.E., F.ASCE[5]

Abstract: With the recent advances in the biogeotechnics field and specifically microbially induced calcite precipitation (MICP), cone penetration testing (CPT) has become a valuable tool to overcome the challenges associated with intact sampling of improved soils, evaluate the spatial extent and magnitude of the applied MICP treatment, and assess the consequential improvement of engineering properties. Although the CPT cone tip resistance (q_c) can effectively monitor the improvement of densified clean sands, no relationship exists to estimate cementation and strength parameters in MICP-treated sands. This paper proposes a relationship between the apparent cohesion (c) stemming from the MICP-induced cementation bonds at particle contacts and the change in tip resistance Δq_c in initially loose sands. To develop a broadly useful correlation, available experimental CPT data in biocemented soils were used to guide computation simulations using a direct axisymmetric model of cone penetration in biocemented sands. The CPT numerical model uses the finite-difference method with a rezoning algorithm for large-deformation problems along with the Mohr-Coulomb constitutive model. The biocemented sand was characterized by Mohr-Coulomb strength parameters and an elastic shear modulus informed by shear-wave velocity measurements (V_s). The correlation parameters of interest were identified (c, q_c, and V_s), and results of the numerical simulations were validated against available experimental data. Once validated, the numerical simulations were extended to different initial conditions, and the trends between parameters of interest were analyzed and interpreted. Results from the simulations are consistent with experimental data and show an increase in the cone tip resistance as the cementation level increases. The cementation level is modeled through apparent cohesion and the shear stiffness model parameters, which both increase as the cementation level increases. A linear relationship is proposed between the apparent cohesion and the change in cone tip resistance as a function of the confining stress. **DOI: 10.1061/(ASCE)GT.1943-5606.0002914.**

Introduction

The cone penetration test (CPT) has been increasingly used as a tool for evaluating whether ground improvement is needed and for quantifying whether realized ground-improvement methods are effective. Current ground-improvement methods include, among others, dynamic compaction, vibrocompaction, chemical grouting, and deep soil mixing, all of which are generally energy- and resource-intensive and can have significant impacts on the environment (e.g., Pinske 2011; Raymond et al. 2020). Over the last decade, alternative biomediated ground-improvement methods that use soil microorganisms to induce calcite precipitation or desaturation have emerged. These biomediated ground-improvement methods have received increased interest due to their potential economic advantages (e.g., cost effectiveness) and lower environmental impact (e.g., less invasive and disruptive than traditional methods) (Hall et al. 2022).

Microbially induced calcite precipitation (MICP) is a biomediated ground-improvement method in which active urease enzymes hydrolyze supplied urea and in the presence of sufficient calcium, induce the precipitation of calcite at particle surfaces and contacts (DeJong et al. 2010). These biocementation bonds improve the engineering properties of the treated soil and its mechanical response (e.g., DeJong et al. 2006; Montoya and DeJong 2015; Gomez and DeJong 2017). As a result, biocementation has become an important alternative for mitigation of erosion, slope stability, and earthquake-induced liquefaction hazards.

Previous researchers (Bachus et al. 1981; Frydman et al. 1980; Molenaar and Venmans 1993) highlighted challenges in physical sampling naturally cemented sands due to the destruction of bonds in compression and shear during conventional sampling, and in tension when extracted from the ground. These cementation bonds are important to preserve because they alter the mechanical response of the soil by contributing to an apparent cohesion between soil particles, thereby increasing the strength and stiffness of the soil. Similar to naturally cemented sands, the in situ characterization and posttreatment verification of biocemented sands is challenging due to the disturbance associated with the sampling process. As a result

[1]Graduate Student Researcher, Dept. of Civil and Environmental Engineering, Univ. of California, Davis, CA 95616 (corresponding author). ORCID: https://orcid.org/0000-0002-5675-1554. Email: melkortbawi@ucdavis.edu

[2]Assistant Professor, Dept. of Civil and Environmental Engineering, Portland State Univ., Portland, OR 97207. ORCID: https://orcid.org/0000-0001-5256-0438. Email: dmoug@pdx.edu

[3]Assistant Professor, Dept. of Civil and Environmental Engineering, Univ. of California, Davis, CA 95616. ORCID: https://orcid.org/0000-0001-5494-497X. Email: kziotopoulou@ucdavis.edu

[4]Professor, Dept. of Civil and Environmental Engineering, Univ. of California, Davis, CA 95616. ORCID: https://orcid.org/0000-0002-9809-955X. Email: jdejong@ucdavis.edu

[5]Distinguished Professor, Dept. of Civil and Environmental Engineering, Univ. of California, Davis, CA 95616. ORCID: https://orcid.org/0000-0002-2518-901X. Email: rwboulanger@ucdavis.edu

Note. This manuscript was submitted on February 1, 2022; approved on July 7, 2022; published online on September 8, 2022. Discussion period open until February 8, 2023; separate discussions must be submitted for individual papers. This paper is part of the ***Journal of Geotechnical and Geoenvironmental Engineering***, © ASCE, ISSN 1090-0241.

of sampling challenges and design conservatism, the improved strength-deformation behavior of cemented sands is rarely considered in design. Furthermore, sampling may not be representative given the variable conditions (e.g., changes in density, confining stress, and microstructure with depth) present in field applications. To overcome these challenges, geophysical and CPT tests provide near-continuous in situ measurements with depth that allow for a more direct characterization of posttreatment biocementation.

Despite sand biocementation becoming an increasingly viable ground-improvement approach (e.g., Esnault Filet et al. 2016) and overcoming the challenges of sampling cemented sands for testing, relationships between their strength properties and in situ test data remain largely uncharacterized. This is largely due to the limited availability of in situ characterization data and complementary strength data. A comprehensive database for biocemented soils is still under development, but when sufficiently populated, it will benefit researchers in biogeotechnics and the geotechnical community by (1) extending the knowledge from artificial biocementation processes to similar natural cementation processes where soil characterization may be improved despite high costs and limited available methods for soil sampling, (2) developing tools to characterize soils that may have greater resistance to certain natural hazards (e.g., erosion or liquefaction) than current practice can assess, and (3) transitioning construction to more sustainable ground-improvement practices without loss of functionality or reliability. Although some relationships with shear-wave velocity (V_s), strength parameters (e.g., cohesion and friction angle), and cement content have been recently published (e.g., Cui et al. 2017; Hoang et al. 2020), a relationship between CPT cone tip resistance q_c and apparent cohesion has not been developed at this time.

The goals of this study are to enable the verification of field biocementation treatment through CPT testing and relate CPT-measured q_c to strength properties of initially loose MICP-treated sands. The connection between the field-measured CPT q_c as the end-of-construction quality assurance and control (QA/QC) and a strength parameter like cohesion will provide a project-specific basis for either simplified strength-based analyses or for constitutive model parameters used in more advanced numerical analyses. These numerical analyses may include the design of ground-improvement techniques, the evaluation of present site conditions, and/or the post-disaster remediation of sites following a hazardous event. To this end, this paper investigates the relationship between the change in cone tip resistance (Δq_c) due to cementation and the apparent cohesion (c) for initially loose biocemented sands. It also proposes a mechanistic approach for synthesizing data from numerical cone penetration simulations validated against large-scale and field-scale experiments, and additional parametric simulations with varying cementation levels and confining stresses.

Fig. 1 conceptually illustrates the approach followed while the following sections describe the various data sources and analysis components. First, the published data from two experiments (a large-tank experiment and a centrifuge test) with CPT q_c and V_s measurements were collected ("Cone Penetration Resistance for Biocemented Sands" section). Second, numerical simulations under similar conditions were performed to reproduce the experimental results by varying the input parameters to the model. The simulation results were then validated against the experimental data. Once validated for the confining pressures from the experiments, the simulations were extended to higher confining stresses, and the trends were analyzed and interpreted in order to fit a relationship between the input parameter to the Mohr-Coulomb constitutive model c and the output from the cone penetration model q_c. The following sections describe this approach in greater detail.

Although other approaches have been followed for the simulation of cone penetration in cemented sands ("Cone Penetration Numerical Simulations" section), the present approach provides a valuable tool in synthesizing data that are validated against the experiments. Without disregarding the complexity of the actual mechanisms during cone penetration, the simplicity of the Mohr-Coulomb model is still preferred at this time. Results from laboratory tests on biocemented sands have been used to directly map to how biocementation changes Mohr-Coulomb model parameters. This process provides a strong experimental basis and guidance for parametric studies for this modeling work. The Mohr-Coulomb constitutive model used here with a modified secant shear modulus and a nondegrading cohesion for the cemented sands still allows for a reasonable approximation of the constitutive behaviors due to two competing mechanisms: (1) the nondegrading cohesion inhibiting dilation, which is offset by (2) the enhanced dilation of cemented sands. However, the authors understand that the actual mechanisms during cone penetration are more complex due to the degradation of the biocementation and its effects.

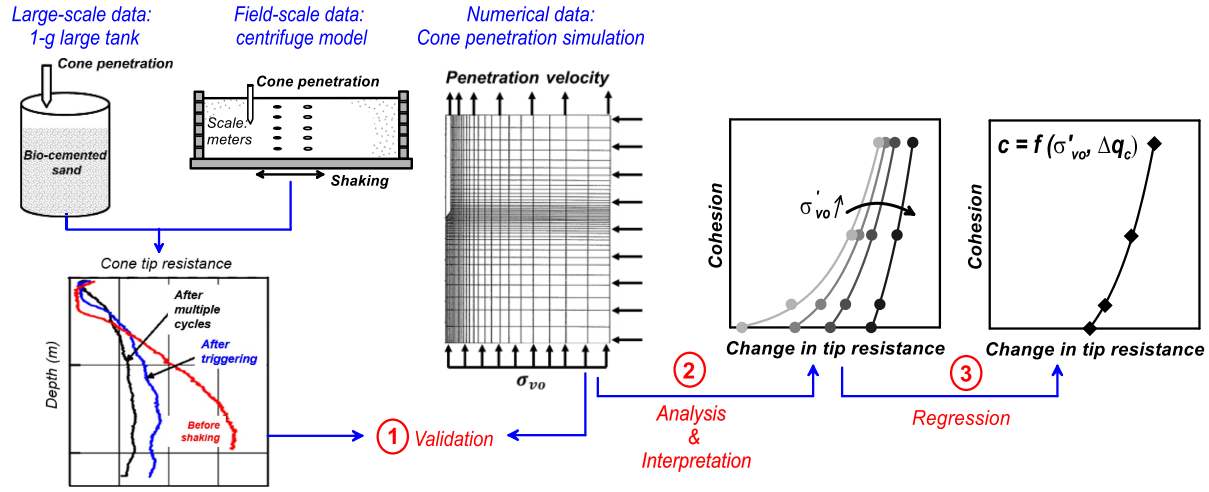

Fig. 1. Proposed approach for the development of a $\Delta q_c - c$ relationship for biocemented sands from experimental and numerically synthesized data.

J. Geotech. Geoenviron. Eng., 2022, 148(11): 04022098

Cone Penetration Resistance for Biocemented Sands

Two published experiments evaluated the use of CPT as a site characterization tool for biocemented sands. These experiments are briefly summarized here because their data sets will be used in subsequent sections to validate the simulated q_c under similar conditions.

Large-Scale Tests

Gomez et al. (2018) treated two 1.7-m-diameter tank specimens at a relative density D_R of 45% with MICP to assess the effect of biocementation on CPT and shear-wave velocity (V_s) measurements. Two biological treatment approaches were used (stimulation and augmentation, one in each tank) to investigate the influence of differences in the biological treatment on the spatial distribution of the cementation. They found that this variation did not significantly affect the magnitude and spatial distribution of biocementation. Thus, for our purposes, data sets from both tanks will be used.

Pretreatment and posttreatment CPT soundings were performed using a 1.6-cm-diameter cone penetrometer at several locations where the level of cementation varied from light to heavy [Fig. 2(a)]. Light cementation is defined as a soil with $V_s \sim 300$ m/s, and heavy cementation is defined as a soil with $V_s \sim 1{,}200$ m/s (after Montoya et al. 2013). V_s and calcite content by mass, measured at the same locations, were used to characterize the cementation level, and they were found to have a positive linear relationship. The average confining stress at the sample locations was approximated as 13 kPa. CPT soundings reported the tip resistance q_c. The q_c values were not corrected for excess pore-water pressures because drained conditions were expected to prevail due to the low cone penetration velocity and the high permeability of biocemented sands. Gomez et al. (2018) have provided more details on the biological treatments and the experimental setup.

Comparing pretreatment and posttreatment CPT data showed that q_c increased with the increase of soil calcite content and V_s (i.e., the level of cementation), with more significant increases in q_c occurring at higher calcite contents. A strong correlation between soil calcite content and V_s has been previously established (e.g., Gomez and DeJong 2017; Gomez et al. 2018; Darby et al. 2019). At lower calcite contents (i.e., less than 3%), increases in q_c were less significant, probably due to the insensitivity of the cone to low levels of cementation. This limitation of the CPT was overcome by V_s measurements, which, due to their nondestructive nature, are sensitive to even the smallest changes in particle bonding.

Data sets from this study were also analyzed within the K_G framework ("Model Validation" section), which was proposed by Schneider and Moss (2011) for cemented and aged soils and is based on the small-strain (Rix and Stokoe 1991) and large-strain characteristics (Eslaamizaad and Robertson 1997) using parameters from field testing. This analysis was done to evaluate the relationship between V_s and normalized cone tip resistance (q_{c1N}) of biocemented sands relative to naturally cemented soils ("Soil Model

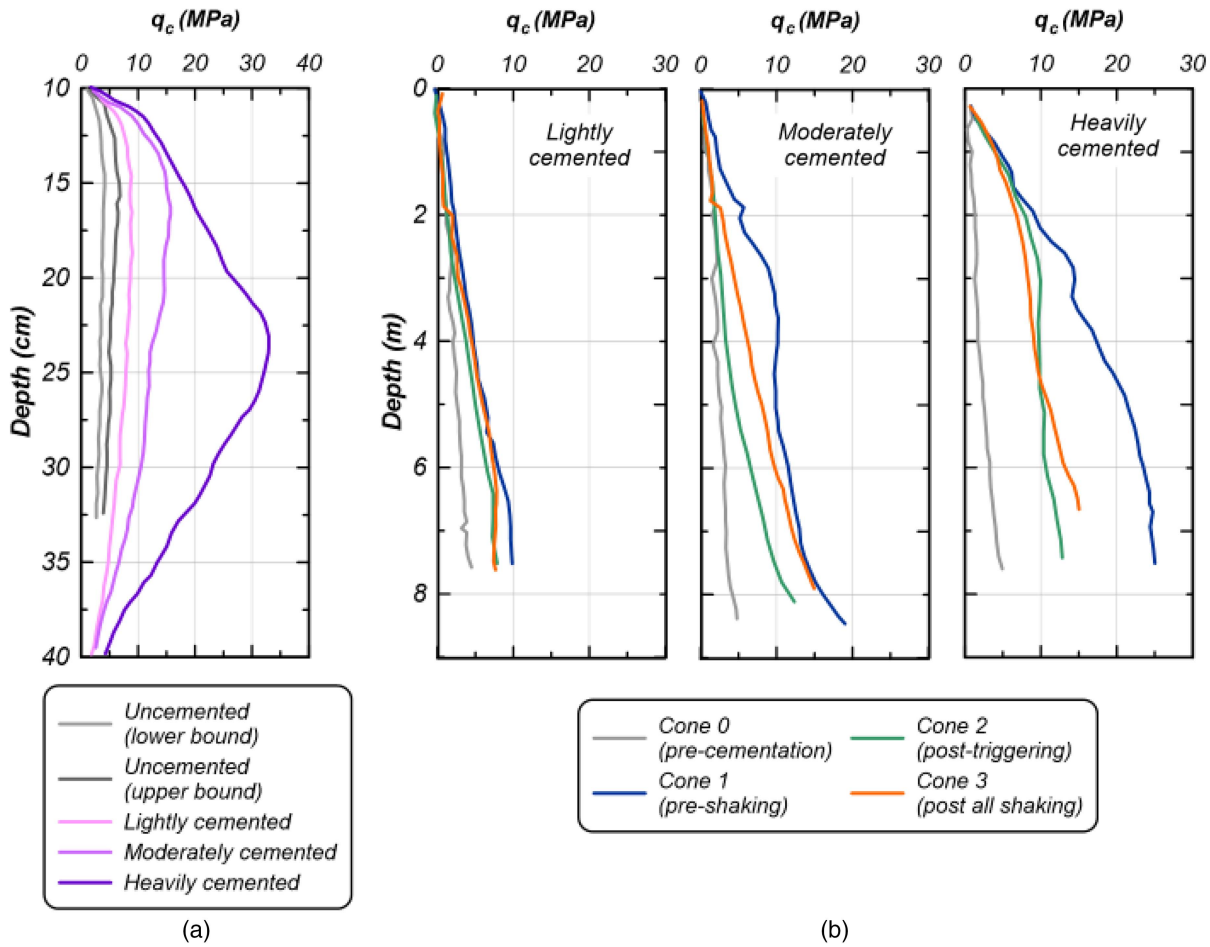

Fig. 2. Cone penetration profiles from (a) large-tank experiment (data from Gomez et al. 2018); and (b) centrifuge model test (data from Darby et al. 2019) showing an increased cone tip resistance before [plots (a and b)] and after [only plot (b)] triggering of liquefaction.

J. Geotech. Geoenviron. Eng., 2022, 148(11): 04022098

Calibration" section). The K_G boundary values were found to reasonably capture the distinction between uncemented and cemented sands.

Centrifuge Model Tests

Darby et al. (2019) performed a set of centrifuge model tests on MICP-treated Ottawa sand at a relative density D_R of 38% and different levels of cementation (i.e., light, medium, and heavy cementation defined based on V_s measurements). Control tests on clean sands at loose and dense states were first performed, and then the biocementation process was induced in loose centrifuge models. All models were spun to a centrifugal acceleration of $80g$ (middepth confining stress was approximated at 35 kPa) and subjected to 9–16 shaking events with acceleration amplitudes ranging from $0.02g$ to $0.55g$. Similar to the large-tank experiment, calcite content measurements, pretreatment and posttreatment CPT soundings, and bender element V_s measurements were combined to assess the effect of biocementation on the cone penetration resistance and the stiffness of the treated specimens. This study also investigated the effect of biocementation on the liquefaction resistance and the postshaking cementation degradation [Fig. 2(b)], which are outside the scope of the present work but shown here for completeness.

The present work focuses on the measured q_c prior to shaking, whereas the Darby et al. (2019) centrifuge study focused specifically on dynamic responses. More details on the experimental setup and postshaking behaviors have been given by Darby et al. (2019). Compared with the pretreatment CPT profiles, posttreatment CPT profiles showed an increase in q_c as the level of cementation increased, due to the filling of void space with the cementation and thus the presence of the bonding between the particles. Measured q_c increased from a middepth value of 2.3 MPa for the uncemented loose model to 4.6, 9.9, and 17.8 MPa for the lightly, moderately, and heavily cemented models, respectively, with an effective vertical stress at middepth ranging from 32 to 36 kPa. These increases in q_c corresponded to increases in V_s and calcite contents in all models and appeared to be linearly correlated to the increase in calcite content, as reported by Gomez et al. (2018) at $1g$ and 13 kPa confinement.

Cone Penetration Numerical Simulations

The availability of CPT data pretreatment and posttreatment is crucial for verifying that ground improvement was achieved. However, there are currently no available methods to relate changes in CPT measurements to mechanical properties of the improved soil, which limits the utility of such data. The mechanical properties of initially loose MICP-treated sands have been increasingly investigated. Research on lightly cemented sands (Puppala et al. 1995; Lee et al. 2011) and on biocemented sands (Burbank et al. 2013; Gomez et al. 2018; Darby et al. 2019) has reported that cementation results in an increase in the cone tip resistance and sleeve friction and a decrease in the friction ratio due the pronounced increase in tip resistance compared with the sleeve friction. This increase in q_c is a direct representation of the increase in strength of the cemented sand, which is mostly attributed to the cohesive bonds. These studies indicated that changes in CPT data can be related to changes in soil mechanical properties due to biocementation.

Researchers (DeJong et al. 2010; Feng and Montoya 2016; Nafisi et al. 2020) have shown that biocementation increases the initial shear stiffness ($G_{\max}$), peak strength (τ_{pk}), and dilative tendencies of treated sands while suppressing the initial contractive behavior due to the presence of the cementation bonds. This results in improved strength properties such as increased cohesion and friction angle. These improvements degrade after the accumulation of plastic strains and the sheared treated sand loses the cementation bonds (El Kortbawi et al. 2022b).

CPT-based relationships are advantageous because the improved strength-deformation behavior is difficult to measure accurately in the laboratory due to sampling challenges. As a result, there is a lack of understanding of how changes in CPT data relate to changes in soil strength properties. Due to the lack of CPT data coupled with conventional laboratory testing of biocemented sands, there is a gap in the understanding and quantification of the strength properties of these biocemented sands, such as apparent cohesion. To address this issue, a numerical direct cone penetration model is used herein.

Simulations of cone penetration in cemented sands have been recently performed by Schweiger and Hauser (2021) and Rakhimzhanova et al. (2021). Schweiger and Hauser (2021) simulated undrained cone penetration in cemented clayey silt using the particle finite-element method (PFEM) and the clay and sand model (CASM) for structured soil. Large deformations due to the cone penetration were handled by the PFEM, whereby frequent remeshing was performed in deformed regions. The numerical model consisted of a rigid cone penetrating a saturated soil at constant velocity. At approximately 25 to 30 cone radii, stationary values of tip resistance and pore pressures were obtained. Structured soils were represented by overconsolidated soils in the CASM constitutive model due to the similarities in their behaviors. The results of the simulations confirmed that before the degradation of the cementation, the cone tip resistance and pore pressures increased with the level of cementation whereas they decreased after the degradation. The trends in the results in terms of changes in pore pressure, undrained shear strength, and cone correction factors were analyzed by Hauser and Schweiger (2021).

Rakhimzhanova et al. (2021) utilized the discrete-element method (DEM) to simulate constant-rate vertical cone penetration in cemented sandstone. The cemented sandstone was represented by frictional elastic spheres with different bond strength values. The results of the simulations were then compared with the published Soil Behavior Type (SBT) classification system based on CPT, demonstrating the utility of numerical cone penetration simulations for relating in situ data to cemented sand properties.

For the present study, cone penetration numerical simulations were validated against existing data and subsequently parametrically performed to produce data for development of a relationship between Δq_c and c, accounting for its dependence on confining stress. Simulations were performed in the explicit finite difference (FD) program Fast Lagrangian Analysis of Continua (FLAC) version 8.1 (Itasca 2019) with the Mohr-Coulomb constitutive model. The cone penetration model has been used in previous studies (e.g., Moug 2017; Moug et al. 2019a, b) and has been validated against laboratory tests. Although the present work and Schweiger and Hauser (2021) used a similar approach in terms of remeshing regions around the cone with large deformations, the tools used (FD versus PFEM, respectively) for the simulation of the cone penetration and the characterization of the cemented soil (Mohr Coulomb versus CASM, respectively) differed. The present work and Rakhimzhanova et al. (2021) also used different tools (FD versus DEM, respectively) and approaches (mesh moving up versus penetrometer moving down, respectively). Despite these differences, the aforementioned studies have similar trends in their findings.

Axisymmetric Cone Penetration Model

The direct axisymmetric cone penetration model (Fig. 3) simulated the steady-state penetration of a standard cone with a 3.57-cm diameter (10-cm^2 cone area) into a soil column using a user-defined

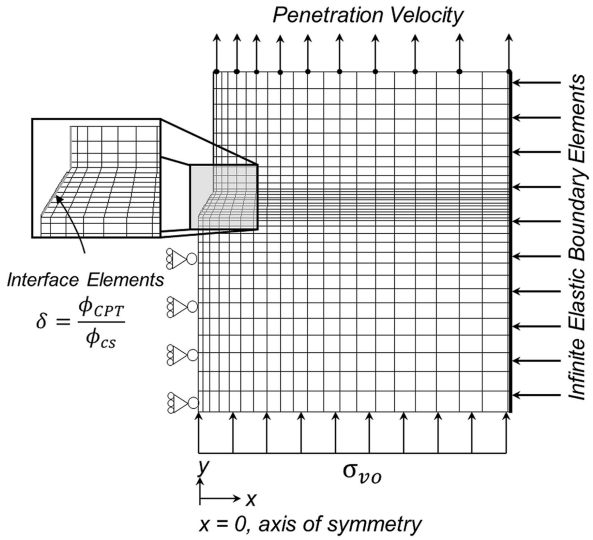

Fig. 3. Geometry and boundary conditions of the numerical cone penetration model in FLAC. (Reprinted from Moug 2017, with permission.)

Arbitrary Lagrangian Eulerian (ALE) algorithm coupled with FLAC's Lagrangian formulation that allows for large deformations (Moug 2017; Moug et al. 2019a). The model was developed to simulate penetration at large depths such that the cone's self-weight and ground surface effects can be neglected. The model was initialized with stress and material properties for a wished-in-place cone at the depth of interest. The penetration was then simulated until a steady-state stress distribution, pore pressure, and tip resistance prevailed, which was approximately 25 cone diameters of simulated penetration (Lu et al. 2004).

Boundary conditions simulated soil flowing upward relative to a stationary cone (i.e., soil flows from the bottom of the model and exits at the top). The far-field total vertical stress was applied at the bottom boundary, a penetration velocity of 0.02 m/s was applied at the top boundary, and an infinite elastic boundary condition was assumed for the right radial boundary, which is far away from the cone to prevent boundary effects. The axisymmetric boundary to the left imposed no displacement in the x-direction for the soil node at the tip of the cone and constrained vertical movement due to the rigidity of interface elements in this direction. The other soil nodes along the cone face and the shaft could deform parallel to the boundaries of the cone. The mesh near the cone face was highly discretized, and the adjacent soil zones were connected by Mohr-Coulomb interface elements obeying the Mohr-Coulomb friction criterion.

The interface coefficient of friction (the ratio of the interface friction angle and the soil's critical state friction angle) represents the friction along the cone face and ranges from 0 to 1 for a perfectly smooth and a perfectly rough cone, respectively. An interface coefficient of friction equal to 0.60 was used for these simulations, which is consistent with the value used for simulated cone penetration in sand by Moug et al. (2019b). The soil zone sizes increase following a power distribution away from the cone. Large deformations of the model geometry, which will concentrate near the cone tip and shoulder, can lead to numerical instability and hence were accommodated with an ALE algorithm, which performs grid rezoning and model property remapping throughout the penetration depth. Details of the ALE algorithm and the model's implementation have been given by Moug (2017) and Moug et al. (2019b). Initial stress conditions corresponded to a normally consolidated K_o condition. Drained conditions were imposed by minimizing the pore-water bulk modulus.

Soil Model Calibration

Mohr-Coulomb, an elastic-perfectly plastic model, is used for simulating penetration in cemented sands due to its simplicity and its applicability to soils with cohesion (e.g., Cui et al. 2017; Nafisi et al. 2020). The calibration of the Mohr-Coulomb constitutive model was guided by the aforementioned experimental data and other bench-scale tests data (e.g., triaxial and direct simple shear tests), previous research on the mechanical behavior of biocemented and naturally cemented sands (El Kortbawi et al. 2022b), and empirical correlations developed hereafter. Mohr-Coulomb model parameters were assigned to capture the drained penetration in uncemented and biocemented sands.

Similar to sands, drained conditions prevail in biocemented sands due to their open structure reflected by the modest changes in hydraulic conductivity after cementation (Gomez and DeJong 2017). Literature on cemented sands (e.g., Dupas and Pecker 1979; Saxena et al. 1988) also suggested that although strength parameters (all in effective stress terms), cohesion c, and friction angle ϕ, are affected by cementation, changes in friction angle are of secondary importance and the main contributor to the improvement in the behavior is the apparent cohesion term c. This hypothesis has been corroborated by a sensitivity analysis on the friction angle using the cone penetration model, not included here for brevity (El Kortbawi et al. 2022a).

Furthermore, the dilation angle ψ was not activated in the simulations because preliminary calibrations suggested an overestimation in the tip resistance. This overestimation is most likely due to the double counting of the cementation effects through a nondegrading cohesion and an enhanced dilatancy occurring simultaneously. Consequently, apparent cohesion is the primary parameter for study, whereas the friction angle ϕ and the dilation angle ψ were held constant at 30° (midrange and typical value for silica sands) and 0° (restricted dilation to compensate for the nondegrading cohesion with large deformations), respectively.

Due to the interconnection between strength and stiffness for biocemented sands, a relationship relating a strength parameter, namely apparent cohesion c, and a stiffness parameter, namely V_s, on the element level enables the estimation of the unknown apparent cohesion for the large-scale experiments. Previous research on biocemented sands (e.g., Simatupang et al. 2018; Nafisi et al. 2020) characterized a coupled interaction between strength and stiffness in which both entities increase postcementation; however, initial shear stiffness increases faster and more significantly relative to strength. This mechanism is represented by a linear relationship between apparent cohesion (c) and the change in shear-wave velocity (ΔV_s) due to the contribution of the cementation. Linearity was corroborated by the trends discussed previously in the large-scale and centrifuge test findings.

The data points with c and V_s measurements from triaxial test data on biocemented sands (O'Donnell et al. 2017; Nafisi et al. 2020) were fitted with a linear relationship. The latter was then applied to the field V_s measurements obtained during the experiments in Figs. 2(a and b) to obtain cohesion estimates. Then, the large-scale experimental data with the cohesion estimates were divided into six bins with cohesions from 0 to 50 kPa, in increments of 5 or 10 (0–5 kPa: 2 data points, 5–10 kPa: 3 data points, 10–20 kPa: 5 data points, 20–30 kPa: 7 data points, 30–40 kPa: 11 data points, and 40–50 kPa: 2 data points). This was done to reduce the scatter obtained by fitting through all data points. The average of each bin was obtained and is plotted in Fig. 4 to give a continuous

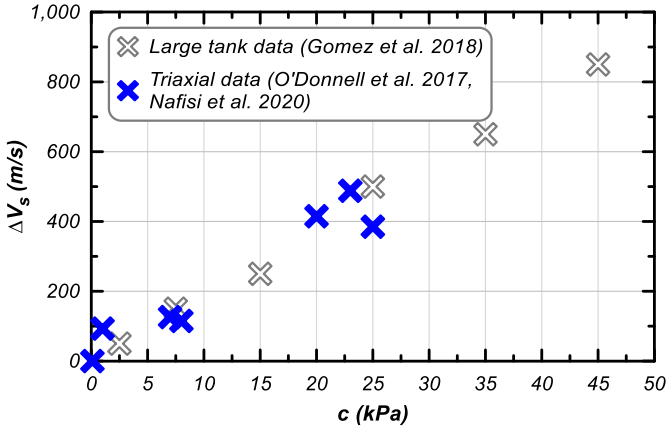

Fig. 4. Relationship between apparent cohesion and change in V_s due to the cementation using large-tank data from Gomez et al. (2018) and triaxial data from O'Donnell et al. (2017) and Nafisi et al. (2020).

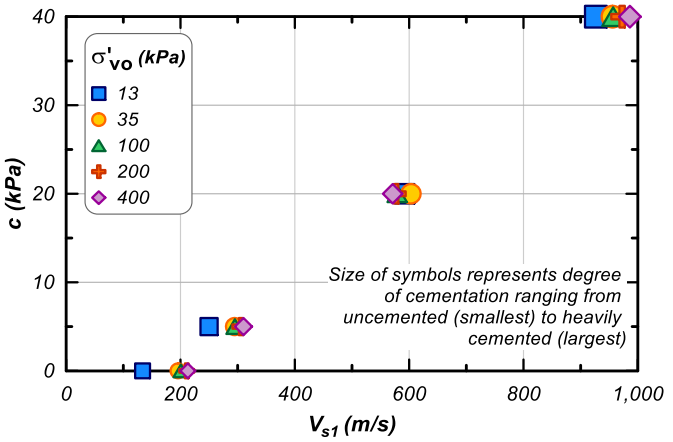

Fig. 5. Normalization of cemented shear-wave velocity V_s across the various confining stresses, resulting in apparent cohesion c and normalized shear-wave velocity V_{s1} pairs similar across all simulations.

Table 1. Mohr-Coulomb input parameters for CPT simulations through cemented sands under various confining stresses

		σ_v' (kPa)				
c (kPa)	ΔV_s (m/s)	13 kPa	35 kPa	100 kPa	200 kPa	400 kPa
		V_s (m/s)				
0	0	80	150	200	250	300
5	95	175	245	295	345	395
20	378	458	528	578	628	678
40	756	836	906	956	1,006	1,056

relationship between cohesion and ΔV_s. Thus, the relationship between apparent cohesion and change in shear-wave velocity becomes

$$\Delta V_s = 18.9c \tag{1}$$

where c = apparent cohesion (kPa); and ΔV_s = change in shear-wave velocity (m/s) due to the contribution of the cementation. The cohesion term used in Eq. (1) and in the rest of the paper refers to the change in cohesion from an initially cohesionless sand ($c = 0$) due to the effects of the cementation. In the absence of bench-scale or field testing, Eq. (1) can be used to provide a rough estimate of the cohesion term directly from the change in shear-wave velocity; however, the data fitted by this equation are limited and hence, other means of estimation are recommended to cross check the estimated c ("$\Delta q_c - c$ Relationship" section).

Based on collected experimental data (El Kortbawi et al. 2022b) and the developed correlation [Eq. (1)], Mohr-Coulomb input parameters for the cone penetration simulations were chosen and are summarized in Table 1. Values for apparent cohesion range from 0 (uncemented) to 40 kPa (moderately heavily cemented). The confining stresses included (1) 13 kPa, representing the operating confining stress for the CPTs pushed in the large tanks from Gomez et al. (2018), (2) 35 kPa representing the operating confining stress for the CPTs pushed in the centrifuge model from Darby et al. (2019), and (3) 100, 200, and 400 kPa in order to expand the parametric space of the simulations to operating field conditions. The values of V_s for uncemented sands (first row in Table 1) are either reported in the experiments (for 13 and 35 kPa) or estimated for 100 (Lee et al. 2022), 200, and 400 kPa.

According to the chosen cohesion values, the change in V_s corresponding to each cohesion value was estimated from Eq. (1), added to the value of V_s for uncemented sand in order to obtain an estimated V_s for cemented sands, and then checked for normalization across the various confining stresses. For consistent sand properties across the different levels of stress, a stress-corrected V_{s1} [Eq. (2)] is estimated using the correction proposed by Andrus and Stokoe (2000)

$$V_{s1} = V_s\left(\frac{P_a}{\sigma_v'}\right)^n \tag{2}$$

where V_s =shear-wave velocity (m/s); P_a = atmospheric pressure; σ_v' = overburden stress; and n = stress exponent. The exponent n decreases from 0.25 (for clean sands) to 0 (for rocks) depending on the level of cementation. The literature review by El Kortbawi et al. (2022b) proposed a decreasing trend for the n exponent as the level of cementation increases. In the present work, the values of the n exponent were chosen as 0.25, 0.18, 0.13, and 0.05 for $c = 0$, 5, 20, and 40 kPa, respectively. This choice seems reasonable for the shear-wave velocity selection process. Some scatter was noticeable for the V_s at 13 kPa, which is due to difficulties in the measurement of the initial V_s in the experiment. The normalization shown in Fig. 5 indicates that a similar V_s input was specified depending on the initial stress conditions, and hence the model was initialized with an equivalent level of cementation for different initial stress conditions.

During cone penetration, a failure zone is formed around the penetrometer, which generally results in a plastic region near the cone and an elastic region further away from the cone. Complex soil deformations are induced within the plastic zone, which in turn affect the shear modulus (Teh and Houlsby 1991). The extent of the failure zone largely depends on the soil shear stiffness and strength, represented by its rigidity index. The current framework did not consider the effect of penetration-induced strains on the shear stiffness of deformed elements near the cone tip. At present, the model operates with a single assignment of shear modulus as opposed to accepting a strain-dependent shear modulus that would better represent the stiffness degradation in the failure zone around the cone tip as the cone penetrates (Konrad and Law 1987; Schnaid et al. 1997; Krage et al. 2014). In recognizing that the small-strain shear modulus G_{max} is overly stiff, a reduced shear modulus G_{func} was used as a reasonable approximation of the local shear stiffness for the failure zone around the cone tip (Yi et al. 2012).

To account for shear modulus softening due to large strains around the penetrating cone, a common approach is to reduce the local shear stiffness by a certain factor [Eq. (3)] with respect to the initial small-strain shear modulus $G_{max} = \rho V_s^2$, where ρ is the soil's density and V_s is the shear-wave velocity (Teh and Houlsby 1991; Lu et al. 2004). Although the authors acknowledge the more common nomenclature for small-strain shear stiffness G_o in the CPT-based literature and frameworks, they chose to use the nomenclature G_{max}. The latter is more common in earthquake engineering applications, which are the end-use of the proposed relationship hereafter. The two quantities denote a maximum value of shear modulus and thus, G_{max} is used in the rest of this paper. Hence, the local functional shear stiffness G_{func} is expressed

$$G_{func} = \frac{G_{max}}{F} \tag{3}$$

where G_{func} = functional shear modulus for large-strain problems; G_{max} = initial small-strain shear modulus; and F = reduction factor due to penetration-induced deformations. The reduction factor was chosen for uncemented sands based on the experience of previous researchers and extrapolated to cemented sands by a calibration process as informed by the degradation of G in the response of monotonic drained triaxial tests (Feng and Montoya 2016; Montoya and DeJong 2015). The proposed relationship for the reduction factor F [Eq. (4)] increases with the level of cementation due to the increased brittleness of the cementation at higher levels. This increase in brittleness results in a sharper decrease in stiffness with deformations for higher levels of cementation (El Kortbawi et al. 2022b). Hence, the shear stiffness is more considerably lost at higher cementation, and a higher reduction factor is needed to reflect this mechanism

$$F = 0.15c + 3 \tag{4}$$

The reduction factor F is linearly proportional to the apparent cohesion c (kPa) and is plotted in Fig. 6.

Additional parameters to the axisymmetric model using the Mohr-Coulomb constitutive model are summarized in Table 2 based on input parameters for cemented sands as summarized in Table 1 and on default values for clean sands wherever no information was available for cemented sands.

In what follows, results from the calibration with the functional shear modulus are presented, and the simulated q_c values are compared with the reported ones from the experiments in the $q_c - V_s$ space (e.g., Andrus et al. 2009; Darby et al. 2019) and in the K_G framework (e.g., Rix and Stokoe 1991; Schneider and Moss 2011; Gomez et al. 2018).

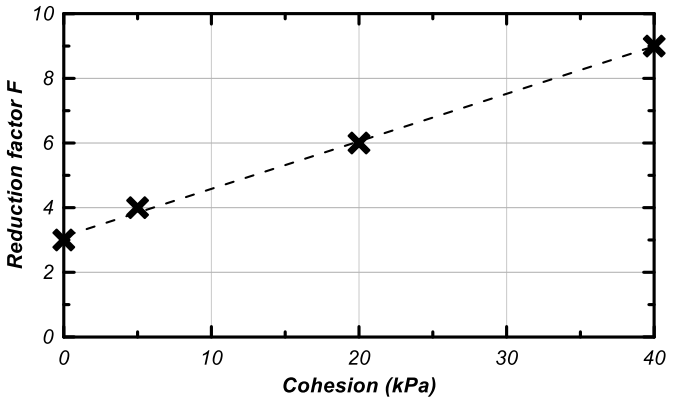

Fig. 6. Proposed relationship for shear modulus reduction factor as a function of the apparent cohesion c, where $c = 0$ and $c > 0$ delineate uncemented and cemented sands, respectively.

Table 2. Calibration of the cone penetration model

Mohr-Coulomb model parameters	Parameter description	Calibration
c	Effective cohesion term (kPa)	Refer to Table 1
ϕ	Effective friction angle (degrees)	30
V_s	Shear-wave velocity (m/s)	Refer to Table 1
ρ	Dry density (Mg/m^3)	1.7
G	Functional shear modulus (kPa)	$G = \frac{G_{max}}{F}$
K_o	At-rest coefficient of lateral pressure	0.5
ψ	Dilation angle (degrees)	0
υ	Poisson's ratio	0.3

Model Validation

To enable the comparison with available experimental data, the focus of the analysis was on the cone tip resistance q_c results, similar to other works (e.g., Puppala et al. 1996; Lee et al. 2010; Schneider and Moss 2011). Simulated tip resistances for effective stresses of 13 and 35 kPa were compared with the reported tip resistances from Gomez et al. (2018) and Darby et al. (2019), respectively.

Fig. 7 represents the simulated and experimental q_c in the q_c-V_s space. The open and solid symbols refer to the experimental and simulated results at different vertical stresses, respectively. The increasing sizes of the symbols delineate the classification of the cementation as uncemented ($V_s \sim 80$–300 m/s for a stress range of 13 to 400 kPa), light ($V_s \sim 170$–400 m/s for a stress range of 13 to 400 kPa), moderate ($V_s \sim 450$–680 m/s for a stress range of 13 to 400 kPa), and heavy ($V_s \sim 830$–$1{,}100$ m/s for a stress range of 13 to 400 kPa), respectively. This facilitates visualization of results not only in the global sense but also on a discretized level-by-level basis.

The simulated q_c values not only fell within the same range as the experimental ones for 13 and 35 kPa but also reasonably mapped the cementation level (i.e., the second smallest symbols from the simulations plot near those from the experiment, delineating a match between the light level of cementation from the

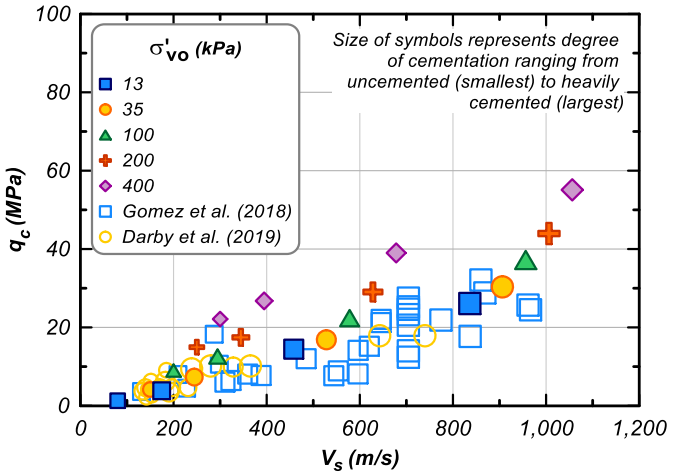

Fig. 7. Comparison between reported experimental (open symbols) and simulated (solid symbols) tip resistances in the $q_c - V_s$ space.

simulation and the experiment). This observation follows a general trend in which an increase in shear-wave velocity results in an increase in tip resistance. The trend extends similarly to higher confining stresses.

Fig. 8 shows the trend between simulated and experimental results in the K_G framework. The parameter K_G is defined as follows:

$$K_G = \frac{G_{\max}/q_c}{q_{c1N}{}^{-0.75}} \tag{5}$$

where K_G = empirical parameter relating stiffness and strength; $G_{\max}$ = initial small-strain shear modulus; q_c = cone tip resistance; and q_{c1N} = stress-normalized cone tip resistance. This framework was adapted by Schneider and Moss (2011) to visualize the relationship between stiffness (originally written in terms of G_o, modified for the purpose of this work) and strength for cemented sands and by Gomez et al. (2018) and Montoya et al. (2021) for biocemented sands. According to the soil classification from Schneider and Moss (2011), the range for cemented sands plots above and to the right of uncemented sands, with the cutoff K_G value between uncemented and cemented soils being 330. With an increase in cementation and age, the parameter K_G [Eq. (5)] is expected to increase proportionally to the level of cementation and perpendicularly to the cutoff ranges.

The small-strain shear stiffness $G_{\max}$ is affected by the coordination number, the characteristics of particle contacts, and the effective stress. It is interpreted from V_s measurements taken during the CPT profiles or from geophysical tests. The tip resistance is a large-strain measurement controlled by a large-strain shear stiffness (or a functional stiffness), soil characteristics (dilation and crushability), and horizontal effective stress. Although these measurements are performed at different zones of the soil, the ratio of q_c to $G_{\max}$ gives reasonable indications on the cementation and geologic age of deposits.

Both the experimental and simulated results reasonably followed the aforementioned trend. A few lightly cemented experimental data plotted under the cutoff K_G value of 330, but most showed the cementation to generate large increases in the K_G value.

In general, the cemented simulated results were plotted above the $K_G = 330$ cutoff and reasonably shifted up and to the right as the apparent cohesion value (i.e., the level of cementation) increased from lightly to heavily cemented. This trend was similarly seen in the experimental work by Montoya et al. (2021) and in the numerical work on cemented sandstone by Rakhimzhanova et al. (2021). Therefore, the penetration model and soil model calibrations are resonably able to capture the effect of biocementation on q_c.

$\Delta q_c - c$ Relationship

Once the simulated tip resistances were validated against the available experimental data sets and engineering correlations, the simulations were extended to higher confining stresses (100, 200, and 400 kPa) to (1) test the validity of the numerical model and thus the trend at relatively higher depths; and (2) extend the parametric space of the simulations and synthesize enough data to establish a relationship between the change in tip resistance due to cementation and apparent cohesion for biocemented sands. The tip resistance of biocemented sands increases with the apparent cohesion (i.e., the level of cementation) and with the confining stress and consequently, the change in the tip resistance due to cementation Δq_c follows the same trend as shown in Fig. 9.

The performed simulations first initialized the confining stress and then applied the cementation. This approach has been chosen to be consistent with how biocementation has primarily been implemented in laboratory tests and how it is expected to be applied in the field. As a result, the cementation bonds formed under the full in situ stress conditions. Therefore, the biocementation treatment was expected to increase the yield stress from the uncemented case at the given confining stress. The magnitude of this increase will depend primarily on the cementation level. Although the effect of cementation becomes less significant at higher levels of stress, it is possible that the yield stress may still affect the $\Delta q_c - c$ relationship (for example, at 500 kPa, which would roughly correspond to a 50-m depth in a saturated sand profile).

Eq. (6) presents a best-fit-line for the apparent cohesion and the change in tip resistance due to biocementation of loose sand. The apparent cohesion increased linearly with the change in tip resistance (Fig. 9), with the slope of the line being a function of the confining stress. A regression analysis using the least-squares method was performed to account for the dependence of the apparent cohesion on the confining stress. It was found that the cohesion is dependent on the square root of the confining stress. The form of this relationship and its dependencies agree with a previously published relationship between tip resistance and cohesion (Lee et al. 2010). The latter was developed from tip resistances obtained from miniature cone penetrometers on gypsum-cemented

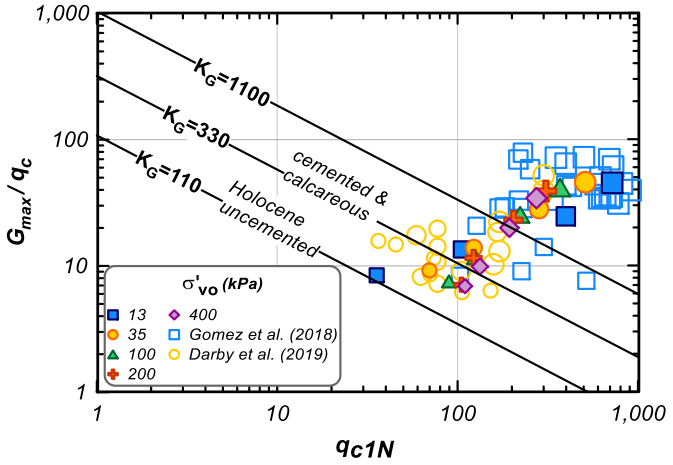

Fig. 8. Comparison between reported experimental (open symbols) and simulated (solid symbols) tip resistances in the K_G framework.

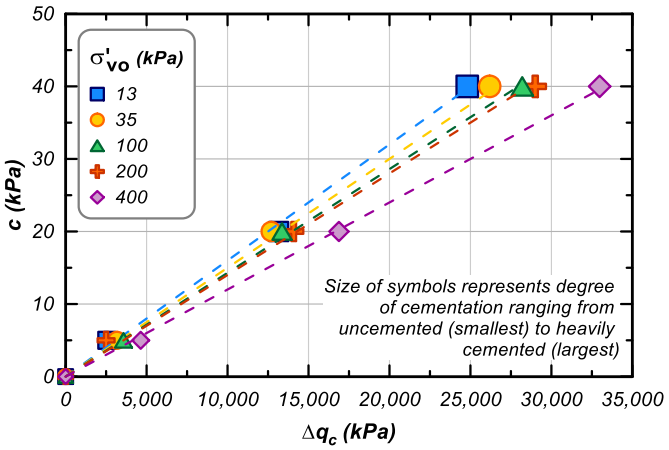

Fig. 9. Trend between cohesion and change in tip resistance from synthesized data and its dependence on confining stress.

J. Geotech. Geoenviron. Eng., 2022, 148(11): 04022098

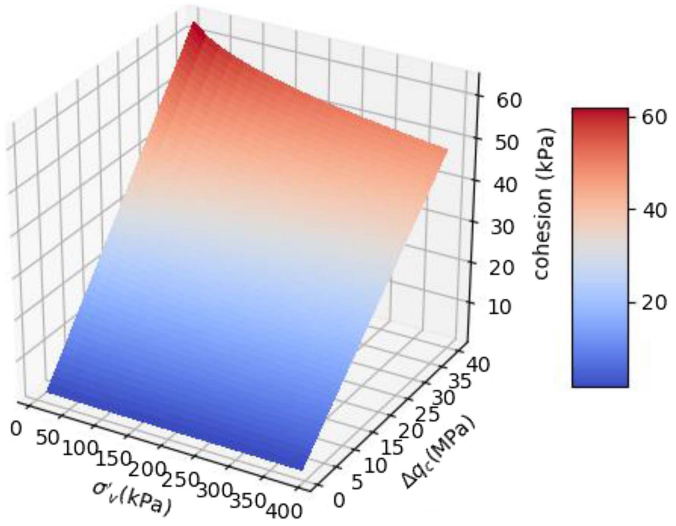

Fig. 10. Three-dimensional surface of the relationship among effective vertical stress, change in cone tip resistance, and cohesion.

sands in a calibration chamber, accompanied by cohesion intercept interpretations from failure envelopes obtained from triaxial tests on the same material

$$c = a \cdot \Delta q_c \tag{6}$$

where

$$a = \frac{1}{587.3 + 12.4 \cdot \sqrt{\sigma'_v}}$$

where c = apparent cohesion; Δq_c = change in cone tip resistance due to cementation; and σ'_v = initial in situ vertical effective stress (all three parameters are in units of kPa for this relationship).

Plotted in a three-dimensional (3D) space, the aforementioned relationship yields the surface shown in Fig. 10. Because the cone tip resistance is largely affected by the strength of the soil, a stronger or cemented soil will exert more resistance to the pushed cone and thus the tip resistance increases as the soil's strength increases. In cemented sands, the latter is mainly attributed to the increase in the apparent cohesion, hence resulting in the upward trend for the apparent cohesion.

The confining stress also plays a major role in the soil's resistance and increase in strength. As the confining stress increases, the soil's strength increases, resulting in an increased cohesion. Although the ranges of tip resistances and vertical effective stresses may be comparable to dense clean sands, the developed relationship is only applicable to initially loose ($D_R = 30\% - 40\%$) MICP-treated sands contributing to a change in tip resistance due to the cementation.

Discussion

The cone penetration model using the Mohr-Coulomb constitutive model enables simulations that cover a range of soil properties and confining stresses to be performed, which is helpful in extending the analysis beyond the limited experimental data for cone penetration measurements in biocemented sands. The Mohr-Coulomb model can reasonably capture the elastic-plastic behavior of biocemented soils in the failure zone near the cone tip through defining the failure envelope with a cohesion intercept and a peak friction angle. Moreover, the Mohr-Coulomb model allows focus on two of the primary factors affecting the cone tip resistance in cemented sands: cohesion and stiffness. Cone tip resistance, and by extension strength, is largely affected by these two factors, but at different rates, which is reflected by Eq. (1). Although the application of a theoretical linear elastic-perfectly plastic continuum model with constant parameters to soil conditions with strain-dependent parameters is fundamentally challenging, the approximation with a functional modulus provides useful predictions of the cone tip resistance (Schnaid et al. 1997).

In the same line of thought and due to the Mohr-Coulomb formulation, the present analyses also assumed a cohesion intercept that remains constant during the cone penetration. Consequently, the dilation angle is not activated to compensate for the reduction in the cohesion intercept due to bond degradation upon shearing with the simultaneous increase in dilatancy due to changes in fabric and particle shape and angularity. This approximation works for the present data set and provides reasonable tip resistances. In addition, it was assumed that steady-state penetration was achieved and drained conditions were preserved during the cone push due to the open structure of biocemented sands and the slight reductions in hydraulic permeabilities from clean sands (Gomez and DeJong 2017). Although the Mohr-Coulomb model provides a reasonable approximation of the mechanisms in biocemented sands, it is understood that the actual mechanisms around the tip are more complex due in part to the degrading effects of the biocementation.

The approach used to develop the $\Delta q_c - c$ relationship consisted of the validation of the simulated cone tip resistances against those reported from two experimental programs on biocemented sands at different confining stresses. Once the tip resistances at 13 and 35 kPa gave reasonably consistent values compared with the experimental ones, the simulations were extended to higher confining stresses and shear stiffnesses, guided by laboratory data at these higher levels. As experimental results at higher confining stresses become available, the tip resistances corresponding to these stresses (100, 200, and 400 kPa) can be further validated. Thus, the $\Delta q_c - c$ relationship presented in this paper is valid for the range of parameters it was developed for. Confining stresses range from 13 to 400 kPa, cohesions range from 0 (uncemented) to 40 kPa, and shear-wave velocities are proportional to the cohesion values.

It is envisioned that the proposed correlation will facilitate the evaluation of biomediated ground improvement at treated sites. Once the treatment process is done, it is recommended that a seismic CPT or a CPT coupled with geophysical tests is performed for the quality assurance and control of the achieved ground improvement. These in situ tests provide a cone tip resistance profile and V_s measurements, respectively. The latter may be used for the quality control of the spatial distribution of the treatment over large areas of the site, whereas the former may be specified to locations of the site where structures and their foundations are expected. Therefore, the response of the foundation bearing soil is crucial for the numerical modeling and design of said foundation and structure, which leads to the importance of the estimation of strength parameters and specifically the apparent cohesion of the treated soil.

Eqs. (1) and (6) provide two fundamentally connected variables (ΔV_s and Δq_c) for the estimation of the apparent cohesion in biocemented sands. Although the estimated values may differ due to the limited body of data used for the fitting of these relationships, the equations can be employed to cross-check their respective results, and an average of the two estimates can be used to determine the apparent cohesion assigned to the constitutive law in the numerical model. Current practices neglect the inevitable presence of cementation in natural deposits due to the lack of understanding of the behavior of cemented sands and/or the inability to characterize them. Often this results in overly conservative designs and higher construction costs. Although this work primarily applies to

biocemented sands, an overlooked benefit is the ability to extend these findings to naturally cemented sands because biocementation is thought of as a proxy to natural cementation in the lab.

Conclusions

This paper proposed a relationship between increases in cone tip resistance Δq_c and apparent cohesion for loose biocemented soils. This relationship was developed through the application of an existing axisymmetric cone penetration model using Mohr-Coulomb constitutive model calibrations. The improvement in the behavior of biocemented sands was attributed to the presence of cementation bonds characterized by an apparent cohesion value, hence the application of the Mohr-Coulomb constitutive model. The axisymmetric model was first calibrated and validated against control tests on clean sands, and then used to estimate cone tip resistances in biocemented sands for a range of cohesions and confining stresses. A simple linear relationship was found between the cohesion and the change in shear-wave velocities for biocemented sands based on available laboratory data on MICP-treated specimens.

Due to the large shear strains imposed on biocemented soils during cone penetration, there are likely compensating effects of reduction in cohesion and increase in dilatancy. The axisymmetric cone penetration model with the Mohr-Coulomb constitutive model using varying functional shear stiffness moduli yielded realistic tip resistances when compared with field data at confining stresses of 13 and 35 kPa. Additional simulations across the parametric space (e.g., varying cementation level and confining stress) led to the development of a proposed relationship between cohesion and the change in cone tip resistance for biocemented sands. Although the ranges of tip resistances and vertical effective stresses may be comparable to dense clean sands, the developed relationship is only applicable to initially loose ($D_R = 30\%$–40%) MICP-treated sands contributing to a change in tip resistance due to the cementation. This relationship mathematically describes the causality between soil strength (in the case of biocemented sands, mainly attributed to cohesion) and tip resistance creating a bridge between a parameter common to modelers and one common to practitioners, respectively. It remains that lab tests could supplement CPT soundings to fully characterize the strength parameters of biocemented sands for design.

Data Availability Statement

Some or all data, models, or code that support the findings of this study are available from the corresponding author upon reasonable request.

Acknowledgments

This material is based upon work primarily supported by the National Science Foundation (NSF) under NSF Award No. EEC-1449501. Any opinions, findings and conclusions, or recommendations expressed in this material are those of the authors and do not necessarily reflect those of the NSF.

References

Andrus, R. D., H. Hayati, and N. P. Mohanan. 2009. "Correcting liquefaction resistance for aged sands using measured to estimated velocity ratio." *J. Geotech. Geoenviron. Eng.* 135 (6): 735–744. https://doi.org/10.1061/(ASCE)GT.1943-5606.0000025.

Andrus, R. D., and K. H. Stokoe II. 2000. "Liquefaction resistance of soils from shear-wave velocity." *J. Geotech. Geoenviron. Eng.* 126 (11): 1015–1026. https://doi.org/10.1061/(ASCE)1090-0241(2000)126:11(1015).

Bachus, R. C., G. W. Clough, N. Sitar, N. Shafii-Rad, J. Crosby, and P. Kaboli. 1981. *Behavior of weakly cemented slopes under static and seismic loading conditions*. John A. Blume Earthquake Engineering Center Rep. No. 44. Stanford, CA: Dept. of Civil and Environmental Engineering, Stanford Univ.

Burbank, M., T. Weaver, R. Lewis, T. Williams, B. Williams, and R. Crawford. 2013. "Geotechnical tests of sands following bioinduced calcite precipitation catalyzed by indigenous bacteria." *J. Geotech. Geoenviron. Eng.* 139 (6): 928–936. https://doi.org/10.1061/(ASCE)GT.1943-5606.0000781.

Cui, M.-J., J.-J. Zheng, R.-J. Zhang, H.-J. Lai, and J. Zhang. 2017. "Influence of cementation level on the strength behaviour of bio-cemented sand." *Acta Geotech.* 12 (5): 971–986. https://doi.org/10.1007/s11440-017-0574-9.

Darby, K., G. Hernandez, J. T. DeJong, R. W. Boulanger, M. G. Gomez, and D. W. Wilson. 2019. "Centrifuge model testing of liquefaction mitigation via microbially induced calcite precipitation." *J. Geotech. Geoenviron. Eng.* 145 (10): 04019084. https://doi.org/10.1061/(ASCE)GT.1943-5606.0002122.

DeJong, J. T., M. B. Fritzges, and K. Nüsslein. 2006. "Microbially induced cementation to control sand response to undrained shear." *J. Geotech. Geoenviron. Eng.* 132 (11): 1381–1392. https://doi.org/10.1061/(ASCE)1090-0241(2006)132:11(1381).

DeJong, J. T., B. M. Mortensen, B. C. Martinez, and D. C. Nelson. 2010. "Bio-mediated soil improvement." *Ecol. Eng.* 36 (2): 197–210. https://doi.org/10.1016/j.ecoleng.2008.12.029.

Dupas, J., and A. Pecker. 1979. "Static and dynamic properties of sand-cement." *J. Geotech. Eng. Div.* 105 (3): 419–436. https://doi.org/10.1061/AJGEB6.0000778.

El Kortbawi, M., K. Ziotopoulou, J. T. DeJong, and D. M. Moug. 2022a. "Effect of sand bio-cementation on cone tip resistance: A numerical study." In *Proc., 5th Int. Symp. on Cone Penetration Testing*. Balkema, Netherlands: CRC Press.

El Kortbawi, M., K. Ziotopoulou, M. G. Gomez, and M. Lee. 2022b. *Mechanical behavior of bio-cemented sands: State review of experimental and numerical developments*. Berlin, Germany: Springer.

Eslaamizaad, S., and P. K. Robertson. 1997. "Evaluation of settlement of footings on sand from seismic in-situ tests." In *Proc., 50th Canadian Geotechnical Conf.*, 755–764. Richmond, VA: BiTech Publishers.

Esnault Filet, A., I. Gutjahr, J. Mosser, L. Sapin, and K. Ibrahim. 2016. "A novel grouting process for the reinforcement of low permeability soils with the use of biocementation by biocalcis." In *Proc., 19th Southeast Asian Geotechnical Conf. & 2nd AGSSEA Conf.* Pathum Thani, Thailand: Asian Institute of Technology.

Feng, K., and B. M. Montoya. 2016. "Influence of confinement and cementation level on the behavior of microbial-induced calcite precipitated sands under monotonic drained loading." *J. Geotech. Geoenviron. Eng.* 142 (1): 04015057. https://doi.org/10.1061/(ASCE)GT.1943-5606.0001379.

Frydman, S., D. Hendron, H. Horn, J. Steinbach, R. Baker, and B. Shaal. 1980. "Liquefaction study of cemented sand." *J. Geotech. Eng. Div.* 106 (3): 275–297. https://doi.org/10.1061/AJGEB6.0000933.

Gomez, M. G., and J. T. DeJong. 2017. "Engineering properties of biocementation improved sandy soils." In *Proc., Grouting 2017*, 23–33. Reston, VA: ASCE.

Gomez, M. G., J. T. DeJong, and C. M. Anderson. 2018. "Effect of biocementation on geophysical and cone penetration measurements in sands." *Can. Geotech. J.* 55 (11): 1632–1646. https://doi.org/10.1139/cgj-2017-0253.

Hall, C., E. Kavazanjian, L. Van Paassen, S. Kamalzare, and D. Parmantier. 2022. "Techno-economic assessment of liquefaction mitigation by microbially induced desaturation." In *Proc., 2021/2022 ASCE Lifelines Conf.* Reston, VA: ASCE.

Hauser, L., and H. F. Schweiger. 2021. "Numerical study on undrained cone penetration in structured soil using G-PFEM." *Comput. Geotech.* 133 (May): 104061. https://doi.org/10.1016/j.compgeo.2021.104061.

Hoang, T., J. Alleman, B. Cetin, and S. Choi. 2020. "Engineering properties of biocementation coarse- and fine-grained sand catalyzed by bacterial cells and bacterial enzyme." *J. Mater. Civ. Eng.* 32 (4): 04020030. https://doi.org/10.1061/(ASCE)MT.1943-5533.0003083.

Itasca. 2019. *Finite Lagrangian analysis of continua*. Minneapolis: Itasca.

Konrad, J. M., and K. T. Law. 1987. "Undrained shear strength from piezocone tests." *Can. Geotech. J.* 24 (3): 392–405. https://doi.org/10.1139/t87-050.

Krage, C. P., N. S. Broussard, and J. T. DeJong. 2014. "Estimating rigidity index (Ir) based on CPT measurements." In *Proc., 3rd Int. Symp. on Cone Penetration Testing (CPT14)*, 727–735. Geneva, Switzerland: CPT'14 Organizing Committee.

Lee, M., H. Choo, J. Kim, and W. Lee. 2011. "Effect of artificial cementation on cone tip resistance and small strain shear modulus of sand." *Bull. Eng. Geol. Environ.* 70 (2): 193–201. https://doi.org/10.1007/s10064-010-0312-0.

Lee, M., M. G. Gomez, M. El Kortbawi, and K. Ziotopoulou. 2022. "Effect of light biocementation on the liquefaction triggering and post-triggering behavior of loose sands." *J. Geotech. Geoenviron. Eng.* 148 (1): 04021170. https://doi.org/10.1061/(ASCE)GT.1943-5606.0002707.

Lee, M. J., Y. M. Choi, M. T. Kim, and W. J. Lee. 2010. "Evaluation of cementation effect of sand using cone resistance." In *Proc., 2nd Int. Symp. on Cone Penetration Testing*, edited by P. K. Robertson and P. W. Mayne. Geneva, Switzerland: CPT'10 Organizing Committee.

Lu, Q., M. F. Randolph, Y. Hu, and I. C. Bugarski. 2004. "A numerical study of cone penetration in clay." *Géotechnique* 54 (4): 257–267. https://doi.org/10.1680/geot.2004.54.4.257.

Molenaar, N., and A. A. M. Venmans. 1993. "Calcium carbonate cementation of sand: A method for producing artificially cemented samples for geotechnical testing and a comparison with natural cementation processes." *Eng. Geol.* 35 (1–2): 103–122. https://doi.org/10.1016/0013-7952(93)90073-L.

Montoya, B. M., and J. T. DeJong. 2015. "Stress-strain behavior of sands cemented by microbially induced calcite precipitation." *J. Geotech. Geoenviron. Eng.* 141 (6): 04015019. https://doi.org/10.1061/(ASCE)GT.1943-5606.

Montoya, B. M., J. T. DeJong, and R. W. Boulanger. 2013. "Dynamic response of liquefiable sand improved by microbial-induced calcite precipitation." *Géotechnique* 63 (4): 302–312. https://doi.org/10.1680/geot.SIP13.P.019.

Montoya, B. M., J. Do, and M. A. Gabr. 2021. "Distribution and properties of microbially induced carbonate precipitation in underwater sand bed." *J. Geotech. Geoenviron. Eng.* 147 (10): 04021098. https://doi.org/10.1061/(ASCE)GT.1943-5606.0002607.

Moug, D. M. 2017. "Axisymmetric cone penetration model for sands and clays." Ph.D. dissertation, Dept. of Civil and Environmental Engineering, Univ. of California, Davis.

Moug, D. M., R. W. Boulanger, J. T. DeJong, and R. A. Jaeger. 2019a. "Axisymmetric simulations of cone penetration in saturated clay." *J. Geotech. Geoenviron. Eng.* 145 (4): 1–13. https://doi.org/10.1061/(ASCE)GT.1943-5606.0002024.

Moug, D. M., A. B. Price, A. M. Parra Bastidas, K. M. Darby, R. W. Boulanger, and J. T. DeJong. 2019b. "Mechanistic development of CPT-based cyclic strength correlations for clean sand." *J. Geotech. Geoenviron. Eng.* 145 (10): 1–13. https://doi.org/10.1061/(ASCE)GT.1943-5606.0002101.

Nafisi, A., B. M. Montoya, and T. M. Evans. 2020. "Shear strength envelopes of biocemented sands with varying particle size and cementation level." *J. Geotech. Geoenviron. Eng.* 146 (3): 04020002. https://doi.org/10.1061/(ASCE)GT.1943-5606.0002201.

O'Donnell, S. T., E. Kavazanjian, and B. E. Rittmann. 2017. "MIDP: Liquefaction mitigation via microbial denitrification as a two-stage process. II: MICP." *J. Geotech. Geoenviron. Eng.* 143 (12): 04017095. https://doi.org/10.1061/(ASCE)GT.1943-5606.0001806.

Pinske, M. A. 2011. "Life cycle assessment of ground improvement methods." Master's thesis, Dept. of Civil and Environmental Engineering, Univ. of California, Davis.

Puppala, A. J., Y. B. Acar, and M. T. Tumay. 1995. "Cone penetration in very weakly cemented sands." *J. Geotech. Eng.* 121 (8): 589–600. https://doi.org/10.1061/(ASCE)0733-9410(1995)121:8(589).

Puppala, A. J., Y. B. Acar, and M. T. Tumay. 1996. "Low strain dynamic shear modulus of cemented sand from cone penetration test results." *Transp. Res. Rec.* 1548 (1): 60–66. https://doi.org/10.1177/0361198196154800109.

Rakhimzhanova, A., C. Thornton, Y. Amanbek, and Y. Zhao. 2021. "Numerical simulations of cone penetration in cemented sandstone." *EPJ Web Conf.* 249 (Jun): 14010. https://doi.org/10.1051/epjconf/202124914010.

Raymond, A. J., A. Kendall, and J. T. DeJong. 2020. "Life cycle sustainability assessment (LCSA): A research evaluation tool for emerging geotechnologies." In *GeoCongress 2020*, Geotechnical Special Publication 320, edited by E. Kavazanjian Jr., J. P. Hambleton, R. Makhnenko, and A. S. Budge, 330–339. Reston, VA: ASCE.

Rix, G. J., and K. H. Stokoe. 1991. "Correlation of initial tangent modulus and cone penetration resistance." In *Proc., 1st Int. Symp. on Calibration Chamber Testing*. New York: Elsevier Science Publishing Co.

Saxena, S. K., K. R. Reddy, and A. S. Avramidis. 1988. "Static behaviour of artificially cemented sand." *Indian Geotech. J.* 18 (2): 111–141.

Schnaid, F., G. C. Sills, J. M. Soares, and Z. Nyirenda. 1997. "Predictions of the coefficient of consolidation from piezocone tests." *Can. Geotech. J.* 34 (2): 315–327. https://doi.org/10.1139/t96-112.

Schneider, J. A., and R. E. S. Moss. 2011. "Linking cyclic stress and cyclic strain based methods for assessment of cyclic liquefaction triggering in sands." *Géotech. Lett.* 1 (2): 31–36. https://doi.org/10.1680/geolett.11.00021.

Schweiger, H. F., and L. Hauser. 2021. "Numerical simulation of CPT with the Clay and Sand Model (CASM) including effects of bonding." In Vol. 1 of *Proc., 16th Int. Conf. of IACMAG*, edited by M. Barla, A. Di Donna, and D. Sterpi, 179–188. Cham, Switzerland: Springer.

Simatupang, M., M. Okamura, K. Hayashi, and H. Yasuhara. 2018. "Small-strain shear modulus and liquefaction resistance of sand with carbonate precipitation." *Soil Dyn. Earthquake Eng.* 115 (Dec): 710–718. https://doi.org/10.1016/j.soildyn.2018.09.027.

Teh, C. I., and G. T. Houlsby. 1991. "An analytical study of the cone penetration test in clay." *Géotechnique* 41 (1): 17–34. https://doi.org/10.1680/geot.1991.41.1.17.

Yi, J. T., S. H. Goh, F. H. Lee, and M. F. Randolph. 2012. "A numerical study of cone penetration in fine-grained soils allowing for consolidation effects." *Géotechnique* 62 (8): 707–719. https://doi.org/10.1680/geot.8.P.155.